Title: Identification of Kinases Activated by Multiple Pro-Angiogenic Growth Factors

Authors: Scott Gruver, Scott Rata, Leonid Peshkin, and Marc Kirschner

Affiliation: Department of Systems Biology, Harvard University Medical School; Boston, MA 02115

ABSTRACT

Antiangiogenic therapy began as an effort to inhibit VEGF signaling, which was thought to be the sole factor driving tumor angiogenesis. It has become clear that there are more pro-angiogenic growth factors that can substitute for VEGF during tumor vascularization. This has led to the development of multi-kinase inhibitors which simultaneously target multiple growth factor receptors. These inhibitors perform better than monotherapies yet to date no multi-kinase inhibitor targets all receptors known to be involved in pro-angiogenic signaling and resistance inevitably occurs. Given the large number of pro-angiogenic growth factors identified, it may be impossible to simultaneously target all pro-angiogenic growth factor receptors. Here we search for kinase targets, some which may be intracellularly localized, that are critical in endothelial cell proliferation irrespective of the growth factor used. We develop a quantitative endothelial cell proliferation assay and combine it with "kinome regression" or KIR, a recently developed method capable of identifying kinases that influence a quantitative phenotype. We report the kinases implicated by KIR and provide orthogonal evidence of their importance in endothelial cell proliferation. Our approach may point to a new strategy to develop a more complete anti-angiogenic blockade.

Introduction

Nearly all tissues require vascularization to maintain homeostasis. Angiogenesis, or the formation of new microvasculature from existing vessels, allows for tissue growth in both normal and pathological circumstances (Potente, Gerhardt, and Carmeliet 2011). A few examples include much of development, wound healing, the formation of the placenta during pregnancy, diabetic retinopathy, and cancer. The complex process involves the coordination of many growth factor-dependent processes including matrix degradation, cell proliferation, motility, morphogenesis, and apoptosis. It was originally thought that vascular endothelial growth factor, or VEGF, was necessary and sufficient for both normal and pathological angiogenesis (Carmeliet 2005). Indeed, blocking VEGF signaling can greatly improve clinical outcomes in the pathological cases of diabetic retinopathy (Crawford et al. 2009) and macular degeneration (Cabral et al. 2017). However, given the somewhat disappointing failure of therapies targeting VEGF in cancer, it appears that, at least in the case of tumor angiogenesis, other growth factors can suffice in the absence of VEGF signaling (Jászai and Schmidt 2019; Khan and Bicknell 2016; Grépin and Pagès 2010).

Renal cell carcinoma (RCC), the most common form of kidney cancer, is one particular cancer where the inhibition of angiogenic signaling is under heavy investigation (Hsieh et al. 2017). RCC provides an instructive example of the importance of VEGF and other angiogenic growth factors. RCC patients treated with VEGFR2 kinase domain inhibitors show moderate increased survival but also eventually develop resistance (Grünwald and Merseburger 2013; Choueiri et al. 2015). Upregulation of other pro-angiogenic growth factors, namely HGF and FGF, have been suggested as potential factors leading to such resistance (Mollica et al. 2019; Zhou et al. 2016). Interestingly, newer generation VEGFR inhibitors which also possess the ability to inhibit other pro-angiogenic factors provide clinical benefit even in patients with total resistance to VEGFR2 mono-inhibition (Choueiri et al. 2015). This has led to calls for the development of a more complete angiogenic blockade (Grünwald and Merseburger 2013). Given the lack of direct comparative studies on the pathways used by different pro-angiogenic growth factors, it is currently unclear what a complete angiogenic blockade would require.

Growth factors have many effects on cells, with perhaps none so well appreciated as their requirement for the passage of untransformed cells through the cell cycle (Gross and Rotwein 2016). Upon the completion of mitosis, if cells in culture find themselves in the absence of growth factors, they exit the cell cycle and enter into a reversible quiescent state (Zetterberg and Larsson 1985). If growth factors are subsequently replaced, cells re-enter the cell cycle, resume growth, duplicate their genome, and divide. The intracellular signaling pathways that transduce the growth factor signal to cell cycle machinery have been intensively studied and many key signaling pathways have been identified for specific growth factors. However, many cell types, such as endothelial cells, respond to multiple growth factors, raising the question of uniqueness and redundancy in growth factor signaling pathways.

In the absence of growth factors, untransformed cells with intact apoptotic pathways also become apoptotic (Sarkar and Mandal 2009; Letai 2006). Thus, the addition of growth factors also serves to suppress pro-apoptotic signaling and cell death. From this perspective, growth factors are often referred to as survival factors (Collins et al. 1994). The mechanisms by which individual angiogenic factors promote passage through the cell cycle and suppress death have been studied to a certain extent. How growth factor signaling pathways comparatively influence cell proliferation is less well studied.

We present here a quantitative assay to study the intracellular signaling responses to proangiogenic growth factors with the goal of identification of shared pathways in primary dermal human microvascular endothelial cells (DMECs). We focus on how growth factors influence proliferation, or the growth of endothelial cell populations. Proliferation is a complex phenotype determined by a balance of birth and death. The assay requires the formulation of a basal proliferation medium in which a low rate of proliferation is achieved through the balance of a low birth rate and a low, but non-zero, death rate. The assay is used to screen ~30 reported angiogenic growth factors for effects on proliferation and identify three that produce a robust increase in proliferation. We then assay the effects of a carefully chosen panel of kinase inhibitors, which when combined with KIR, a recently developed machine learning method (Taranjit Singh Gujral, Peshkin, and Kirschner 2014; Rata et al. 2020; Taranjit S. Gujral et al. 2014), implicates specific kinases as important in DMEC proliferation in response to specific growth factors. Focusing on the intersection of the implicated kinases in each growth factor tested, we identify kinases that are central to endothelial cell proliferation regardless of the growth factor input. Finally, we apply an orthogonal method to contribute to the evidence for the kinases implicated by KIR.

Establishment of a Quantitative Endothelial Cell Proliferation Assay

We wish to create an assay and accompanying analytical framework that will produce quantitative measures of DMEC proliferative response to single purified pro-angiogenic growth factors. This includes generating an experimental system that allows for the passive counting of cells over time, computing proliferation rates and characterizing the proliferative response of DMCEs to pro-angiogenic growth factors. We then use the assay to determine the quantitative effects of a highly characterized set of kinase inhibitors on DMECs' proliferation rate. Inhibitor alteration of the proliferation rate is then fed into KIR analysis, generating a ranked list of kinases with predicted contribution to setting the proliferation rate.

The Experimental System

To create a quantitative, time-lapse assay of proliferation in response to purified growth factor, we labelled the nuclei of dermal microvascular endothelial cells with nuclear-localized mCherry (Fig1A). Imaging of NLS-mCherry-labeled DMECs counterstained with a DNA-binding dye revealed the labelling efficiency to be ~97% (not shown). Using 384-well plates, with a single 4x image, we were able to image the entire population of labeled cells within a well. Expression of the nuclear-localized mCherry offered the ability to use image processing methods to count cells in real-time (FigS1A). Through comparison with manually counted images, we estimated an absolute counting error of 3% (not shown). The counting error from the automated method was independent of density (Fig.S1B). Finally, expression of this nuclear reporter proved to be passive as it did not alter the doubling time when compared to unlabeled parental population (Fig S1C). Therefore, we are able to count cells proliferating *in vitro* in a reliable, non-invasive manner.

Box 1

Cell proliferation, or growth of cell populations, is a combination of cell birth and death. The *per capita* proliferation rate, P, can be defined as the difference between the birth rate, B, and death rate D

$$P = B - D. \qquad \text{Eq.1}$$

It may be worth specifically pointing out some implications of the fact that the proliferation rate is determined by a balance of cell birth and death. On the extreme end of the spectrum where conditions are entirely favorable, the death rate will be zero and $P = B$. Conversely, when conditions do not allow for birth but also lead to death, $P = -D$. In conditions in between these two extremes, any observed proliferation rate can be achieved through a balance of birth and death.

The per capita birth rate has units of births per cell per unit time while the death rate has units of deaths per cell per unit time. As our experimental system allows for the measurement of live and dead cells over time, we wish to obtain estimates of birth and death rates through time-lapse measurements of the number of nuclei and the number of dead cells. To do so, we first define the proliferation rate as:

$$\frac{dN}{dt} = P(t)N(t), \qquad \text{Eq. 2}$$

where $N(t)$ is the number of nuclei at time t and $P(t)$ is the instantaneous proliferation rate. The generality of this simple model is apparent since from it one can arrive at a whole family of commonly applied models of population growth. For example, if $P(t)$ is defined as a constant, say k_P, then equation 2 has the solution of exponential growth:

$$N(t) = N_0\, e^{k_P t} \qquad \text{Eq.3}$$

Where N_0 is the population size at time $t = 0$. Equation 3 well describes many populations, particularly in the early phase of growth (i.e., before density-dependent effects begin to dominate). Likewise, if one assumes a density dependence of the population growth of a specific form, then equation can be solved to yield the logistic growth model.

Since equation 2 depends so strongly on $P(t)$, the issue therefore becomes a matter of discovering what $P(t)$ looks like in our assay. Equation 2 can be rearranged to

$$P(t) = \frac{dN}{dt}/N(t), \qquad \text{Eq. 4}$$

to obtain a useful form for examination of P(t) from the data as everything on the right-hand side is easily observable.

Similarly, we can study the death rate by defining it as

$$\frac{dM}{dt} = D(t)N(t), \qquad \text{Eq. 5}$$

where $M(t)$ is the number of dead cells at time t and $D(t)$ is the time-dependent death rate. Equation 5 can be rewritten in the same manner as equation 2 to reveal a useful formula for the death rate.

$$D(t) = \frac{dM}{dt}/N(t). \qquad \text{Eq. 6}$$

Armed with $P(t)$ and $D(t)$, we can then easily obtain $B(t)$ from Equation 1, i.e.,

$$B(t) = P(t) + D(t)$$

The Proliferative Behavior of Cells in the Experimental System

Next, we examined the proliferative behavior of DMECs after plating in full growth medium. Full growth medium contains 5% FBS and a cocktail of growth factors. Following an approximately 28-hour period of attachment in this rich growth medium (Fig. S1D), the cells entered into a phase of exponential growth (Fig 1B). Proliferation continued exponentially for another 70 hours, deviating only as the confluency reached ~70%. Such exponential growth is expected in a population where there are abundant resources (excess growth factors), and inhibitory crowding effects (contact inhibition) are absent (see Box1). These results also defined the confluency below

which contact inhibition remains insignificant and we were able to directly verify that in the presence of growth factors, the proliferation rate is independent of plating density (Fig, S1E).

Having characterized the proliferative response in the presence of excess growth factors, we next attempted to isolate the proliferative effects of purified growth factors. To accomplish this, we formulated a basal proliferation medium without any exogenous growth factors and significantly reduced serum. The goal of this medium was three-fold: 1.) to increase the dynamic range of the assay by a reduction in the basal proliferation rate compared to that observed in full growth medium, 2.) to achieve specificity through a reduction in background growth factor signaling due to their presence in serum, and 3.) to model the re-entry of resting endothelial cells in vessels into the cell cycle by synchronization of cells in the G0 phase of the cell cycle. Ideally, cells in a basal medium would show little to no net proliferation. We explored the possibility of achieving this goal via titration of serum in a commonly used endothelial basal medium (Zetterberg and Larsson 1985). When the serum content was too low (i.e., < 0.5%) a net loss of cells occurred, suggesting that many cells died from growth factor withdrawal. From these experiments we defined basal proliferation medium (BPM) to contain 1% serum. Comparing the proliferative response of DMECs in BPM (Fig. 1E), where there is very little net increase in the number of cells over time, to full growth medium (Fig. 1B), it is clear BPM offers considerable dynamic range.

To evaluate the effectiveness of BPM in reducing background growth factor-induced pro-proliferative signaling, we sought to physiologically characterize cells cultured in BPM. We compare the effects of full growth medium and BPM on the proliferative signaling state of DMECs (Shiojima Ichiro and Walsh Kenneth 2002; Srinivasan et al. 2009). BPM reduces the phosphorylation state of ERK2, Akt, p90RSK etc. as compared to cells in full growth medium in as little as 24 hours (Fig. S1F). Thus, BPM reduces the background well-appreciated pro-proliferative signaling molecules in endothelial cells.

Resting endothelial cells in a blood vessel, before receiving pro-angiogenic stimuli, would be in a quiescent state, or the so-called G0 phase of the cell cycle. Using DNA-staining for cell cycle analysis and comparing DMECs in full growth medium and in BPM shows that BPM has expected effects on the cell cycle (Fig. 1C). Specifically, in growth medium, the majority of cells are found in G1/G0, but a significant number of cells are in S- and G2/M-phases. At this level of analysis, it is impossible to distinguish between cells in G0 and G1. However, EdU labeling of DMECs in full growth medium shows that within the length of the typical DMEC cell cycle (~28 hours), nearly all cells pass through S-phase suggesting that there are no cells in G0 in growth medium (not shown). In BPM, we see a nearly complete loss of cells in S and G2/M and a concomitant increase in cells (>91%) arrested in G0/G1. As we will show later in the discussion of Fig. 3, we have reason to believe that the 1*N* peak in BPM (Fig 1C, right panel) contains cells in G0. Therefore, BPM offers desirable dynamic range, reduces background pro-proliferative signaling, and isolates DMECs in G0 or a quiescent state.

The realization that DMECs not only cannot proliferate in low growth factor conditions but in fact die led us to wonder if the overall low proliferation rate in BPM was achieved through a balance of birth and death (see Box 1). To measure dead cells, we optimized the use of the cell-impermeable DNA-binding dye, YOYO1. With this dye, a dead cell can be easily seen as the mCherry signal fades, membrane integrity is lost, cellular DNA is exposed, and the YOYO1 signal appears (see Fig. 1D). The dye is easily detected at low concentrations, stable throughout the timeframe of the assay (not shown) and appears to be passive in that it has no effect on proliferation (Fig S1G). Importantly, cell death in BPM was infrequent and occurred in a rather reproducible manner with a cell rounding up and blebbing, followed by death with little further fragmentation and the cell most often remaining attached in place. The exception to remaining attached was an occasional tendency for living, motile cells to adhere to the dead cell body. These favorable features allowed for the quantitation of cell death using YOYO-1.

In BPM, there was a small but reproducible death of cells (Fig. 1E) revealing that the low level of net proliferation in BPM is due to a balance between the birth and death rate. Since DMECs are a primary cell isolate rather than a transformed cell line, we assume them to be more sensitive to growth factor levels and more susceptible to pro-apoptotic signals. Furthermore, we have shown that culture in BPM reduces pro-proliferative/pro-survival signaling (Fig S1F). Give these facts and the morphological changes seen during cell death (Figure 1D), we hypothesized that the death in BPM was due to apoptosis. The spontaneous cell death in BPM appears to be apoptosis as it can be inhibited by pretreatment with the caspase inhibitor, Q-VD-OPh (Fig. 1F, S1H). As a negative control, pretreatment with necroptosis inhibitor necrostatin was ineffective at blocking cell death in BPM.

In summary, we have generated an experimental system that allows for the quantitative study of *in vitro* endothelial cell proliferation. We can accurately count living and dead cells accurately without considerable impact on proliferative behavior. BPM reduces background pro-proliferative signaling, offers significant dynamic range and models the cell cycle state of endothelial cells in resting blood vessels. Furthermore, BPM creates a state where birth and death are balanced and the effect that growth factors may have on this balance can be examined.

Identification of Growth Factors with Pro-Proliferative Behavior in the Experimental System

Having established an experimental system for studying the proliferation of endothelial cells, we sought to identify growth factors with pro-proliferative activity. Through literature search we identified more than 30 growth factors suggested to be pro-angiogenic. We obtained 33 from commercial sources and tested them in the DMEC proliferative setup described above (Table S1). We were disappointed to see that the vast majority of these reported growth factors had no effect on DMEC proliferation. The source of discrepancy between reported results and our results is not immediately clear but may include differences in endothelial cell isolates. We found that four families of growth factors were capable of increasing proliferation: members of the FGF (FGF1 and 2), VEGF (VEGFA165 and VEGFA145), and EGF (EGF and TGFα) families along with HGF. The effects of EGF were significantly weaker than the others and therefore was not included in subsequent analysis. It must be noted that both FGF and HGF are commonly indicated as sources of resistance to VEGF blockade in many cancers, including RCC (Mollica et al. 2019; Zhou et al. 2016).

Features of Growth Factor-Induced Population Dynamics

Having generated and characterized an experimental system to study the proliferative effects of identified growth factors on DMECs, we sought to determine mathematical definitions for proliferation, birth, and death rates. Although the proliferation rate in full growth medium was constant, it was not immediately clear that the proliferation rate in response to starvation and stimulation with single purified growth factors would behave similarly. The data for each well is quite noisy and the detailed study of the proliferation, birth, and death rates requires numerical differentiation of the noisy data. To limit the effect of applying noise-amplifying numerical process to noisy data, we performed a set of experiments with hundreds of replicates (wells in a 384 well plate) for each condition and applying data smoothing where necessary to generate easily interpretable data. As it is appreciated that such smoothing can affect the exact timing of events, here we focus on a qualitative description of the data and analyses with the intention of using it to arrive at simple definitions for the rates of interest that do not require numerical differentiation.

The number of cells per well (N) in response to addition of purified FGF2 is shown as a function of time in Figure 2A. In contrast to the simple case of exponential growth in full growth medium (Fig. 1B), there appears to be two phases: slow steady growth from the initiation of the experiment to around 24 hours followed by a second phase of more rapid proliferation. The first

phase appears to be largely independent of growth factor concentration while the second phase showed strong dose dependence. At this level it is not clear whether or not the time of entry into the second phase is sensitive to FGF2 concentration.

The number of dead cells per well (*M*) from the same experiment is shown in Fig 2B. It too shows concentration dependence and two phases, albeit on a separate time scale compared to the two phases of net population growth seen in Figure 2A. For dead cells, the first phase is short lived transitioning into the second phase after only ~10 hours.

The plots of *N* and *M* over time reveal intriguing characteristics of the concentration-dependent proliferative behavior of DMECs. Taken alone, however, they do not provide deep insight into the proliferative behavior we isolate in the experimental system developed here. To better understand the proliferative behavior of DMECs following the addition of purified growth factors to BPM, we compute the proliferation, birth, and death rates (see Box 1). In general, the rates of interest could be a function of the density of cells (here called *N*) or the time, *t*.

We suspected that the growth factor dependence of the first phase to be the result of growth factors' rapid effect suppressing apoptosis. Furthermore, the abrupt transition from the first slow phase to the second faster phase was due to the degree of synchrony in the cell cycle introduced by BPM and the time required for cells to re-enter the cell cycle, synthesize DNA, and undergo mitosis. Examination of the birth rate over time showed that, indeed, cells appeared to divide with some degree of synchrony, producing a spike in the birth rate. Meanwhile, the death rate proved to be more-or-less constant over the course of the experiment.

To examine the potential time and density dependence of the endothelial cell proliferation, we computed the proliferation rate and plotted it vs density and time. In contrast to density, where we saw no obvious relationship, there is strong time dependence with the proliferation rate peaking at around 30 hours after the addition of growth factor. The rise and fall of the proliferation rate occurred in a dose-dependent manner and the time of maximum proliferation rate was consistent. It begins around the same time, peaks at the same time, and ends at the same time regardless of growth factor dose. The proliferation rate begins to rise around 20 hours and peaks around 30 hours and returns to low level by 40 hours. The mean cell cycle length of these cells was determined by measurement of the doubling time in complete medium to be 21 hours. We interpret the extra time needed to divide during the first division post growth factor treatment to be the passage of cells from G0 in to G1. Thus, the time dependence of the proliferation rate is a direct consequence of the synchronization of the population in G0.

From here, we considered extracting parameters like the maximum proliferation rate or the time of maximum proliferation rate. The definition of the time-dependent proliferation rate (and more specifically, the scale of the experiment required to clearly see the time dependence) did not allow us to determine these parameters on the scale required to measure the effect of perturbations. We elected to define an apparent proliferation rate that captured the most relevant features of growth factor-induced proliferation.

Dose-Response Behavior to Pro-Angiogenic Growth-Factors

The dose-response behavior of pro-angiogenic growth factors is shown in Figure 3. The proliferation rate (Fig. 3A) shows FGF2 to be the most potent and efficacious at driving proliferation. VEGFA and HGF both shared similar efficacy but VEGFA was slightly more potent in that it could produce measurable effects at lower molar concentrations. Since the proliferation rate is the difference between the birth and the death rate (see Box 1) the proliferation rate alone does not completely characterize the system. Comparing the proliferation rate (Fig. 3A) to the birth and death rates (Fig. 3B and C, respectively) shows a more complete story. Two interesting and related features appear: 1.) given the relatively low magnitudes of the death rates the proliferation rate is mostly governed by the birth rate and 2.) growth factors, even at low

concentrations push the low death rate closer to zero. Thus, the action of growth factors in the assay is two-fold: first they quickly reduce the death rate while initiating the re-entry into the cell cycle leading to a semi-synchronous wave of birth.

Testing a Panel of Kinase Inhibitors

To identify kinases that are used by endothelial cells regardless of the growth factor input, we applied KIR (Rata et al. 2020; Taranjit Singh Gujral, Peshkin, and Kirschner 2014; Taranjit S. Gujral et al. 2014). KIR consists of two steps, first measuring the quantitative effects of 58 kinase inhibitors on proliferation rate in the presence of FGF2, VEGFA, and HGF. The kinase inhibitors used here have been fully characterized against 369 human protein kinases in *in vitro* biochemical assays and have been chosen to provide coverage of the human kinome. The second step uses the biochemical kinase inhibition data with the degree of inhibition of proliferation within a regularized regression framework to identify kinases important for proliferation.

It was qualitatively apparent that some kinase inhibitors, especially at higher concentrations, produced cell death to an extent that greatly exceeded the apoptosis seen in BPM. Examination of the calculated death rates in the presence of kinase inhibitors confirmed that there were in some cases rapid and massive death. In many cases, the proliferation rate was negative, indicating net loss of cells. These scenarios, where it can be assumed that the birth rate is negligible, provide two independent approximations of cell death. Often in these situations, the loss of cells indicated by the loss of nuclei exceeded the independently measured increased number of dead cells, resulting in unrealistic negative birth rates. This indicates a failure of YOYO-1 to accurately reflect cell death in cases of rapid and extensive death. As a result, for the remaining analysis, we focus on analysis of the proliferation rate which is obtained through high confidence counting of labeled nuclei.

Regularization Regression to Identify Universal Kinases

Kinases were identified as the output of regularized regression using the package glmSparseNet (Veríssimo et al. 2018) with the regularization weight alpha set to 0.15 and the kinases were taken as the set of kinases that had nonzero coefficients at the value of lambda with lowest mean-squared error (Figure S2B). A dataset of mRNA expression levels in DMECs (Davis et al. 2018; ENCODE Project Consortium 2012) was used to identify the set of kinases expressed (Figure S2A). This procedure produced a ranked order list of kinases important for proliferation for each of the three growth factors tested. The output is shown in Figure 4A. Most kinases appeared in more than one growth factor indicating a degree of similarity in signaling pathways that drive proliferation in endothelial cells. To reduce the complexity of returned kinases and focus on a subset that might prove an enticing target for a more complete antiangiogenic blockade, we chose to compile the intersection of the kinases from each growth factor (Figure 4B). The identity of the kinases in the intersection of all three growth factors are listed in Figure 4C. The kinases in the intersection proved to be a mix of kinases with well appreciated roles in basal metabolism (IR) or proliferation (AKT2 (Shiojima Ichiro and Walsh Kenneth 2002), CDK6 (Sherr, Beach, and Shapiro 2016), PKACG (Yang et al. 2013), and PEAK1 (Wang et al. 2018)) but also some with understudied roles in proliferation (e.g., DCAMKL2, GRK5/6, and DMPK). Interestingly, the magnitude of the regression coefficient for kinases showed no relationship with the mRNA expression level, suggesting that the method is not simply isolating highly expressed kinases (Figure S3).

Orthogonal Experimental Evidence for Kinases Returned From KIR

We used siRNA to obtain orthogonal evidence that the kinases that were contained within the intersection had impact on the proliferation rate. First, siRNA transfection was optimized for DMECs and the specific plating conditions of the proliferation assay (not shown). We are aware that siRNAs have considerable limitations in this setting for at least two reasons. The first is general to siRNA and is that application of too much siRNA can produce significant off-target effects while too little might obscure real contributions to proliferation. The second is more specific to this system – as DMECs are primary cells, independent confirmation of siRNA-mediated knockdown is not feasible. Overall, we wish to address these limitations using a conservative approach, with the goal of leveraging the assay's reproducibility and quantitative sensitivity to reduce off target effects at the potential expense of on-target effects.

For the first limitation, we aimed to thread this needle by determining the concentration at which siRNAs targeted to each growth factor receptor inhibited the proliferation of DMECs in the presence of its cognate growth factor but not the others. Although there is only one known receptor for HGF (namely MET), the fact that there are four potential FGFRs and three VEGFRs required us to first experimentally determine which receptors are expressed. Via western blot, we identified the receptors expressed to be FGFR1 for FGF2, VEGFR2 for VEGFA, and Met for HGF (Figure S3). We attempted to account for the second limitation by using three siRNAs directed towards each gene of interest and considered the effect to be an average of all three siRNAs.

Using the optimized transfection conditions, we determined the concentration of siRNAs directed toward the expressed growth factor receptors which resulted in a reduction of the proliferation rate in the presence of the cognate growth factor but not the other two. For example, a specific knockdown of FGFR1 would be expected to reduce the proliferation rate of DMECs in the presence of FGF2 but not VEGFA. We found that using 5 nM produced little to no effect while 15 nM produced strong off target effects (not shown). siRNAs directed toward growth factor receptors at 10 nM appeared to generate specific, on-target reductions in proliferation rate while avoiding off-target responses (Figure 5A). Note that for each target, the reductions in the proliferation rate are incomplete, suggesting that we can indeed measure difference using relatively low concentration of siRNA which should limit non-specific effects.

Next, we tested the intersection kinases using three independent siRNAs to each kinase and the effect of knockdown of each gene was taken to be the average of the effect of all three siRNAs. This conservative approach was chosen because of the difficulty in ascertaining the extent of knockdown in limiting numbers of primary cells on the scale necessary for this work. We present the magnitude of each kinase knockdown in Figure 5B as the difference between control and knockdown, or Δk_p. The magnitude of each effect was tested with ANOVA followed by multiple comparisons. Significantly, the knockdown of most, but not all, of the kinases resulted in significant phenotypes as indicated by the asterisks. Again, because of the limitations inherent in siRNA knockdown in this system, we elected to continue our conservative approach and focus on kinases with significant effect in all three growth factors. The results clearly suggest four kinases to be important for endothelial cell proliferation in FGF2, VEGFA, and HGF: AKT2, CDK6, CAMKL2, and PKACG. Of these, three (AKT2, CDK6, and PKACG) are well characterized. The role of the fourth kinase, DCAMKL2, in endothelial cell proliferation has not been studied and is therefore of considerable interest as a new regulator of endothelial cell proliferation and angiogenesis.

We would like to emphasize that while the knockdown of a kinase producing an effect in all three growth factors certainly provides strong evidence for a role in proliferation, we cannot with great confidence exclude the possibility that those that did result in an effect in one or two growth factors (or even those that had no significant effect at all) do not also have a considerable impact on endothelial cell proliferation. For example, it would seem unlikely that the insulin receptor is somehow not important in FGF driven proliferation.

Discussion

Despite the initial disappointment, anti-angiogenic therapy remains an enticing approach to treating cancer, particularly in RCC. Furthermore, given the fact that angiogenesis is critically involved other pathological disorders as well as in wound healing, the desire for a more thorough understanding of the regulation of the process remains high. Here, we present a novel approach for the identification of critical kinases downstream of growth factor receptors.

Using KIR, we identified 19 kinases to be important for endothelial cell proliferation in the presence of multiple bona fide pro-angiogenic factors. Further we also provide evidence using an orthogonal method that four of these 19 are critical for endothelial cell proliferation. One of these four kinases, CDK6, has an inhibitor Palbociclib approved for treatment of cancer. Indeed, some have speculated that at least some of Palbociclib's efficacy is due to an anti-angiogenic effect (Liu, Liu, and Chen 2018; Ehab and Elbaz 2016). This work also indicates the DCAMKL2 as a novel regulator of endothelial cell proliferation. DCAMKL1 and 2 are understudied kinases, with the majority of work being upon DCAMKL1 and its role in cancer (Ferguson et al. 2020), neuronal survival (Nawabi et al. 2015), and maintenance of intestinal crypt cell stemness (Chandrakesan et al. 2017). It will be of interest to further explore the role of DCAMKL2 in endothelial cell biology.

Methods

Growth Factors and Cytokines. All human recombinant growth factors and cytokines were purchased from PeproTech (NJ) and resuspended in the solvent recommended by the manufacturer at 100µg/mL, aliquoted, and frozen until use.

Cloning. The viral transfer plasmid expression a nuclear-localized mCherry was obtained using standard cloning techniques. First, pLVX-EF1α-mCherry-N1 (puro) was digested with EcoRI and NotI. The 8.5kB band representing the backbone of the vector was excised and purified. The nuclear-localized mCherry was digested from pBRY-nuclear mCherry-IRES-PURO (Addgene plasmid 52409) and the ~860bp band was gel purified. The insert was ligated into the pLVX vector overnight at room temperature, transformed into Stbl3 bacteria and plated on LB/ampicillin plates. Colonies were picked, cultured overnight and tested for proper ligation using digestion with EcoRI and NotI. Positive clones were tested be sequencing and the sequence of both the 3X-NLS and mCherry was confirmed to be correct.

Cell Culture, Virus Production, and Viral Transduction. Human Dermal blood microvascular endothelial cells (DMECs) isolated from a single donor were purchased from Lonza (CC-2183). DMECs were cultured in EGM2-MV (Lonza) and passaged using trypsin and trypsin neutralization solution (Lonza). Viruses carrying a gene for the expression of nuclear localized mCherry were produced via triple transfection of HEK-293T cells using FuGENE. The plasmids used were psPAX2, pMDG.2, and pLVX- E1α-NLS-mCherry. Twenty-four hours after transfection, the medium was replaced. For the next 3 days, the supernatant was collected, spun at 500xg to remove large debris and stored at 4C. After all supernatant

was collected, the pooled supernatant was passed through a 0.45 μm filter and transferred to centrifuge and centrifuged for 90 minutes in a SW28 singing bucket rotor. After centrifugation, the supernatant was discarded and the pellet containing concentrated virus was resuspended in 100 μL of PBS. To create a large supply of labeled DMECs, three tubes of purchased DMECs were thawed, counted, plated at 5000 cells/cm^2 and cultured overnight. The next day, purified and concentrated virus was added to the cells at MOI = 5 in medium containing 8 μg/mL polybrene. The next day, the medium was changed, and the cells were cultured continuously, passaged when ~80% confluent until reaching the sixth passage (cells are purchased at passage three). At this point, the cells were trypsinized, pelleted, counted, and resuspended in EGM2-MV supplemented with 10% DMSO at a density of 500,000 cells/mL. The labeled DMECs were aliquoted in 500 uL aliquots and frozen at -80C overnight and then transferred to long term storage in liquid nitrogen. For every experiment presented here, tubes were thawed, viable cells determined and plated at 5000 cells/mL, cultured for 6 days with medium changes before being collected, counted and plated.

Formulation of Basal Proliferation Medium (BPM). BPM contains 0.5% human AB serum (0.5%), insulin, r-Transferrin, 0.5% BSA, hydrocortisone.

The proliferation assay. YOYO-1 iodide was purchased from ThermoFisher (Y3601) and added to BPM immediately before plating cells for the proliferation assay. DyeCycle Green was purchased from ThermoFisher and used as a live cell stain at a final concentration of 10 μM to count living nuclei and determine the labeling efficiency of nuclear mCherry transduction and expression.

Image Analysis for Counting Nuclei and Dead Cells. Time-lapse imaging of DMEC proliferation was done in an IncuCyte ZOOM (Sartorius) with a 4x objective. Nuclei and dead cells were counted using the built-in image analysis capabilities of the IncuCyte ZOOM.

Cell Cycle Distribution and EdU Incorporation. DMECs were plated on poly-L-lysine coated 6 well glass bottom plates at 8,450 cells per cm^2 in either BPM or growth medium (EGM2-MV, Lonza). After 24 hours, cells were fixed with 4% paraformaldehyde in PBS for 10 minutes, permeabilized with 0.1% triton in PBS for 10 minutes, then stained with DAPI (Cell Signaling) for one hour at room temperature. Following staining, cells were washed once with PBS and then imaged immediately on a Nikon at 10x.

For long-term EdU incorporation, we first optimized the concentration of EdU that could be detected but not greatly alter the proliferation rate. We did this by plating cells in varying concentration of EdU in growth medium and fixing after various times. We found that culture in 240 nM EdU for 48 hours less than 5 % reduction of the proliferation rate while being incorporated into ~95% of cells. For experiments, we then plated cells in BPM, and 24 hours later, added EdU with the growth factor or added complete growth medium.

ELISA. Pre-coated ELISA plates were purchased from R&D Systems and performed according to manufacturer instructions. Cell culture supernatants were obtained by plating 600 cells per well in 384 well plates in 60 μL BPM. After 24 hours, 20 μL of BPM containing growth factors at 4x intended final concentration were added. Twenty-four hours following growth factor addition, 60 μL of supernatant was removed from each well and pooled according to growth factor and concentration. The pooled supernatants were then clarified by centrifugation to remove any cell debris and frozen at -20C until all replicates were performed. Supernatants were thawed to room temperature and utilized immediately in the ELISA.

Analysis of kinetic measurements of cellular proliferation and death. We applied the following definitions to calculate per capita proliferation rates for each well:

$$P(t) \approx k_P = \frac{\frac{\Delta N}{\langle N \rangle}}{\Delta t} = \frac{\frac{N(t_{end})-N(t_0)}{N(t_{end})+N(t_0)/2}}{t_{end}-t_0}.$$

Where $N(t)$ is the number of nuclei as a function of time, $\langle N \rangle$ is the average number of nuclei over the experiment, and t_0 and t_{end} is the first and last time points in the experiment. The death rate was defined similarly:

$$D(t) \approx k_D = \frac{\frac{\Delta M}{\langle N \rangle}}{\Delta t} = \frac{\frac{M(t_{end})-M(t_0)}{N(t_{end})+N(t_0)/2}}{t_{end}-t_0}.$$

The birthrates were then calculated as $k_B = k_P + k_D$. These definitions assume that the rates are independent of the overall density and time. Although we show that density is not a critical factor (Figure S1E), the rates are clearly dependent on time (Figure 2). We use these definitions as they are simple to compute and calculation of time-dependent rates were not feasible with the noise inherent in the data.

Kinase Inhibitor Screen

Extensively characterized kinase inhibitors were tested in the proliferation assay in the presence of each of the three growth factors. Inhibitors were tested with four replicates at each of six concentrations, the highest being 5 μM with serial 3-fold dilution.

Kinome Regression (KIR)

Kinome regression was performed as regularized regression using the R package glmSparseNet. The input was the calculated difference between each inhibitor/growth factor combination and the appropriate control (DMSO/growth factor combination) contained on the same plate. The kinase data from the in vitro characterization was filtered according to endothelial cell expression (https:// www.encodeproject.org, identifier: ENCFF110UGQ) using a cutoff of 1.5 arbitrary expression units (see Figure S2). The following parameters were used in the analysis: α = 0.15 and standardize = TRUE.

siRNA Validation of Kinases Identified by KIR.

We tested four different siRNA transfection reagents (RNAiMAX, DharmaFECT 4, for two properties: 1.) To efficiently knock-down a gene of interest and 2.) to have minimal impact on proliferation in the assay. To evaluate transfection efficiency, we used KIF11 which is critical for cytokinesis and when knocked down results in easily scored rounded cells. We found that 1uL/mL of RNAiMAX resulted in 95% rounded cells in while decreasing the proliferation rate by less than 3%. We knocked down kinases using siRNAs from Qiagen (see spreadsheet for the ordering numbers of the siRNAs used) at 10 nM. For transfection, cells were plated in BPM containing YOYO1 in 384 well plates as usual for the proliferation assay. While the cells were adhering, siRNA transfection complexes were formed after a 10-minute incubation and added to the cells with four replicates. Twenty-four hours after plating/transfection, growth factors were added at the following concentrations: FGF2, 1.25 ng/mL; VEGFA, 20 ng/mL, and HGF, 20 ng/mL. The plates were then added to the IncuCyte ZOOM and imaged every two hours for 48 hours. The proliferation rates were extracted as described in the section.

FIGURE LEGENDS

Figure 1. Establishment of the Experimental System. A.) Demonstration of DMEC labeling. Fluorescent image of nuclear-localized mCherry overlaid on a phase contrast image of confluent DMECs. B.) The proliferation of DMECs in full growth medium (dotted line) is exponential (red line is a fitted exponential curve). C.) Cell cycle analysis of DNA ploidy determined by labeling live cells with Hoescht and imaged with a microscope. Full growth medium (left panel) produces a familiar distribution of cells while 24 hours in BPM (right panel) produces far fewer cells in S- and G2/M- phases. D.) Demonstration of YOYO-1 dye to detect dead cells. E.) Example of nuclei (closed circles) and dead cells (open circles) over time in BPM. F.) Cell death seen in BPM can be inhibited by inhibition of caspase activity via 10 μM Q-VD-OPh.

Figure S1. More on the Establishment of the Experimental System. A.) Nuclei can be counted via image processing. The right panel shows a fluorescent micrograph of nuclear mCherry labeled DMCEs, while the center panel shows the mask generated by automated image analysis. The right panel shows the overlay of the two. B.) There is a high degree of correspondence between automated counting (x-axis) and manual counting of nuclei (y-axis). Additionally, the error is apparently independent of density. C.) Labeling DMECs with nuclear mCherry via lentivirus-mediate gene transfer does not alter the doubling time of DMECs. D.) Left panel: Nuclear labeled DMECs produce exponential growth over an interval of time as evidenced by linear relationship between time in hours (x-axis) and the natural logarithm of cell number (y-axis). Right panel: Percent confluence for the same experiment. Note the deviation from exponential growth occurs at ~120 hours or when confluency grows above ~70%. For both panels, solid line is data, dashed line is a fitted exponential curve. E.) The proliferation rate (defined as in main text, section *Features of Growth Factor-Induced Population Dynamics*) is independent over a range of plating densities in the presence of growth factors. F.) Plating DMECs in BPM reduces the phosphorylation of Akt, ERK1/2, and S6 Kinase. G.) YOYO-1, at concentrations as high as 50 nM, have no effect on the proliferation of DMECs. H.) The inhibition of death rate in BPM (defined as in main text, section *Features of Growth Factor-Induced Population Dynamics*) is dependent on the concentration of inhibitor. I.) The death rate in BPM is not inhibited by relevant concentration of the necroptosis inhibitor necrostatin.

Figure 2. Concentration-Dependent Population Dynamics of DMECs in the Presence of Pro-Angiogenic Growth Factors. A.) The number of cells (*N*) over time for four concentrations of FGF2. B.) The number of dead cells (*M*) over time for the same experiment shown in panel A. C.) The proliferation rate, *P*, for the same experiment in panels A and B. D.) The birth rate, *B*, as a function of time. E.) The death rate, *D*, as a function of time.

Figure 3. The dose-response proliferative behavior of DMECs to Three Pro-Angiogenic Growth Factors. The proliferation rate (A), the birth rate (B), and the death rate (C) for FGF2, VEGFA, and HGF over a range of concentrations. Note that the y-axes share the same scale to facilitate comparison of the relative magnitude of each.

Figure 4. Identification of kinases important for the proliferation rate of DMECs in each pro-angiogenic growth factor studied. A.) Plots of the KIR coefficients (i.e., influential kinases) and their magnitudes for each growth factor. B.) Venn diagram revealing the exclusivity and commonalities between each growth factor regarding kinases with influence over proliferation rate. C.) The list of the intersection of kinases implicated in all three growth factors.

Figure S2 Additional data regarding KIR. A.) From left to right we detail the RNA-seq dataset used to identify the set of kinases expressed by DMECs. On the far left is shown the histogram of expression levels

of all 17,698 genes in the dataset. The bimodal nature of the expression data is easily seen and suggests that genes in the first peak with relatively low expression values are not actually expressed while those in the second more broad peak with higher expression values are. Moving rightward, the histogram of the expression of only protein kinase genes (N = 493) is shown. It can be seen that kinases too follow the expected bimodal distribution as seen for all genes. We use these two observations to justify the selection of a threshold for real kinase expression. This threshold was set at 1.5 arbitrary units. Next histogram shows the distribution of the 377 expressed kinases in DMECs. Finally, on the far right we see the histogram of the intersection between expression kinases and KIR kinases, i.e., those for which the compounds have been thoroughly characterized. Thus, we arrive at 265 kinases which could potentially be returned from KIR analysis. This is not the final number as will be detailed next. Note that in Fig. S2A the number of kinases in the RNA-seq dataset is 493. This is 25 shy of the total number of kinases thought to be in the human genome. Of the 25 kinases not in the expression data, five are KIR kinases. To be conservative, we include those kinases in our analysis. B.) Plots of log(λ) vs mean-squared error (MSE) from leave-one-out cross-validation. We used the kinases from the model that minimize MSE (vertical dashed line).

Figure S3 The KIR coefficients plotted against the mRNA expression level. Note the lack of relationship between expression level and magnitude of contribution. It can also be seen that two kinases for which we lack expression data, PEAK1 and PKACG, were returned by the analysis.

Figure 5. Orthogonal Data Supporting the Role of Kinases Return from KIR Analysis. A.) Targeting growth factor receptors with 5 nM of siRNA reduces the proliferation rate of DMECs in the presence of cognate growth factors while minimizing reduction in proliferation in other growth factors. B.) Targeting kinases with siRNA largely agrees with kinases implicated by KIR. Here, effect is defined as the average over all three siRNAs used for each kinase. Error bars are s.e.m. The asterisks indicated $p < 0.05$ from multiple comparison testing.

Figure S4. The identification of relevant growth factor receptors expressed on DMECs via western blotting. There are two VEGF receptors in the genome with kinase activity, VEGFR2 and VEGFR3. DMECs only express VEGFR2. Similarly, there are four FGFRs in the human genome and DMECs only express FGFR1.

FIGURE 1

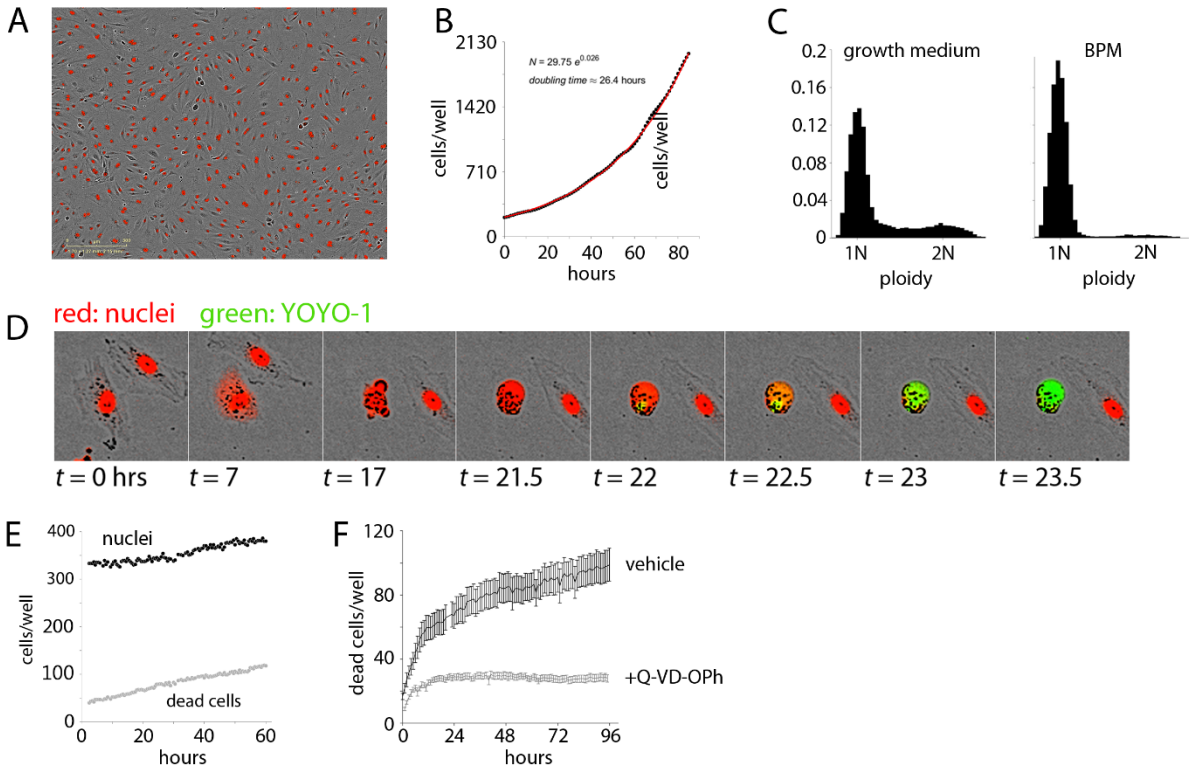
A
B
2130
1420
710
0
cells/well
N = 29.75 e^0.026
doubling time ≈ 26.4 hours
0 20 40 60 80
hours
C
growth medium
BPM
0.2
0.16
0.12
0.08
0.04
0
1N 2N
ploidy
D
red: nuclei green: YOYO-1
t = 0 hrs t = 7 t = 17 t = 21.5 t = 22 t = 22.5 t = 23 t = 23.5
E
nuclei
dead cells
400
300
200
100
0
cells/well
0 20 40 60
hours
F
120
80
40
0
dead cells/well
vehicle
+Q-VD-OPh
0 24 48 72 96
hours

FIGURE 2

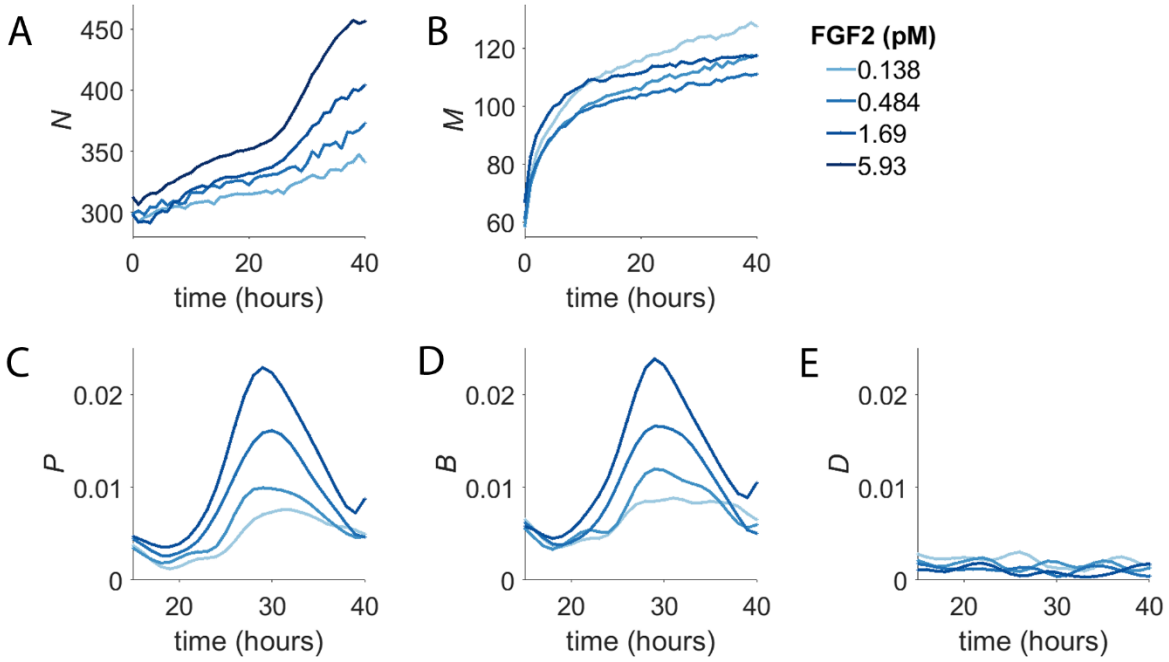
A
450
400
350
300
N
0
20
40
time (hours)
B
120
100
80
60
M
0
20
40
time (hours)
FGF2 (pM)
0.138
0.484
1.69
5.93
C
0.02
0.01
0
P
20
30
40
time (hours)
D
0.02
0.01
0
B
20
30
40
time (hours)
E
0.02
0.01
0
D
20
30
40
time (hours)

FIGURE 3

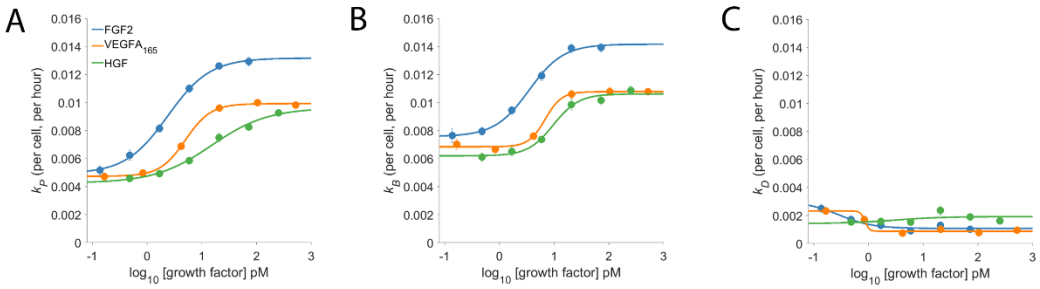
A
B
C
FGF2
VEGFA165
HGF
kP (per cell, per hour)
kB (per cell, per hour)
kD (per cell, per hour)
log10 [growth factor] pM
0.016
0.014
0.012
0.01
0.008
0.006
0.004
0.002
0
-1
0
1
2
3

FIGURE 4

A

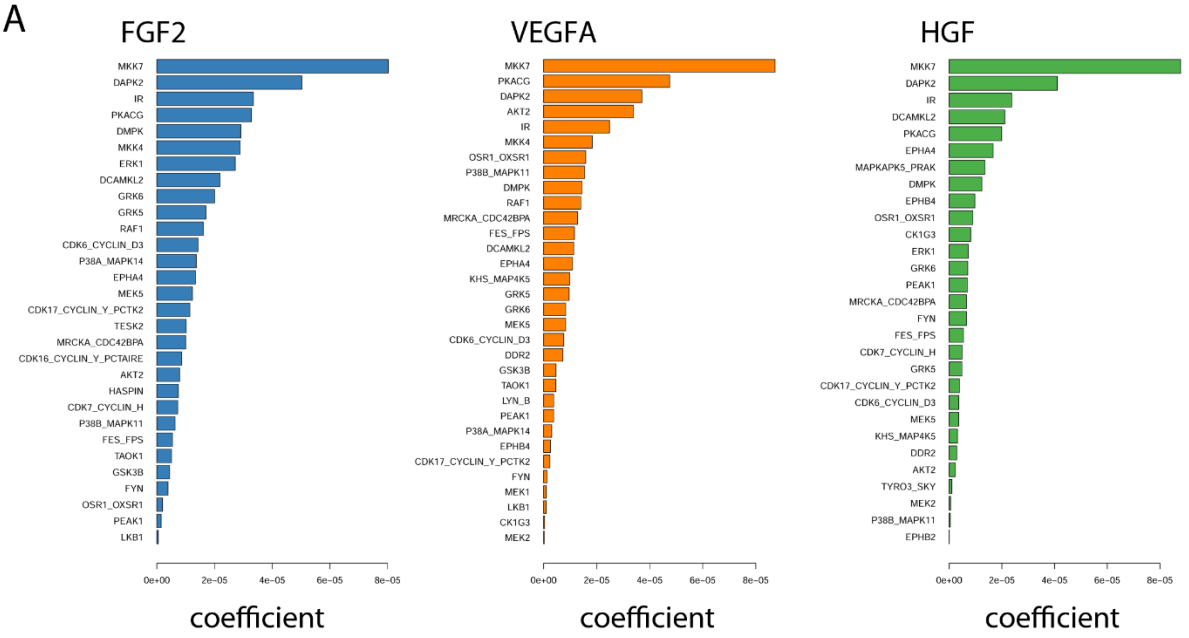

B

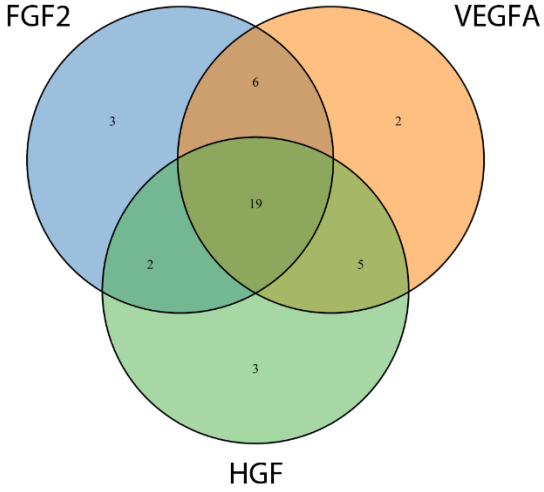

C

AKT2
CDK6/CYCLIN D3
CDK17/CYCLIN Y
DAPK2
DCAMKL2
DMPK
EPHA4
FES/FPS
FYN
GRK5
GRK6
IR
MEK5
MKK7
MRCKA/CDC42BPA
OSR1/OXSR1
PEAK1
PKACG
p38β/MAPK 11

FIGURE 5

A

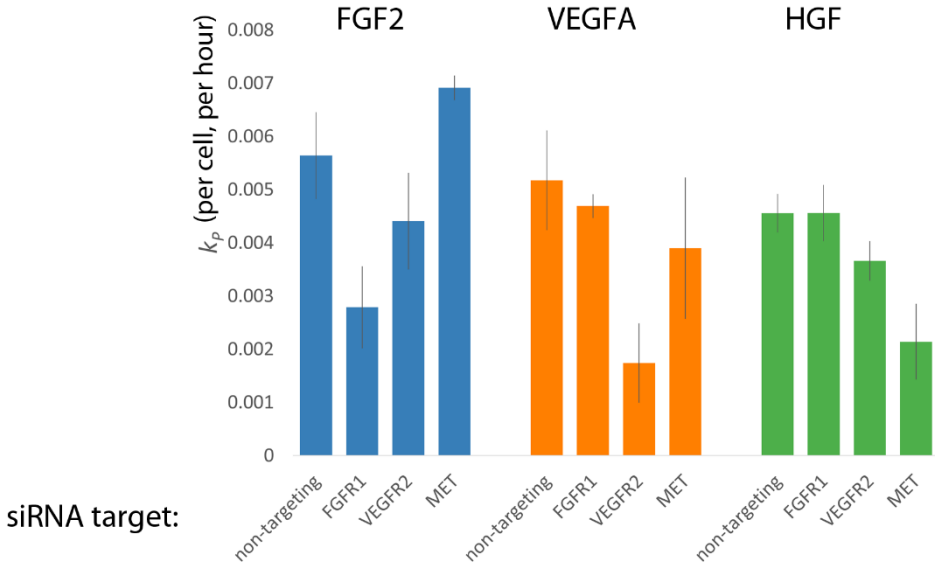
FGF2
VEGFA
HGF
k_p (per cell, per hour)
0.008
0.007
0.006
0.005
0.004
0.003
0.002
0.001
0
siRNA target:
non-targeting
FGFR1
VEGFR2
MET

B

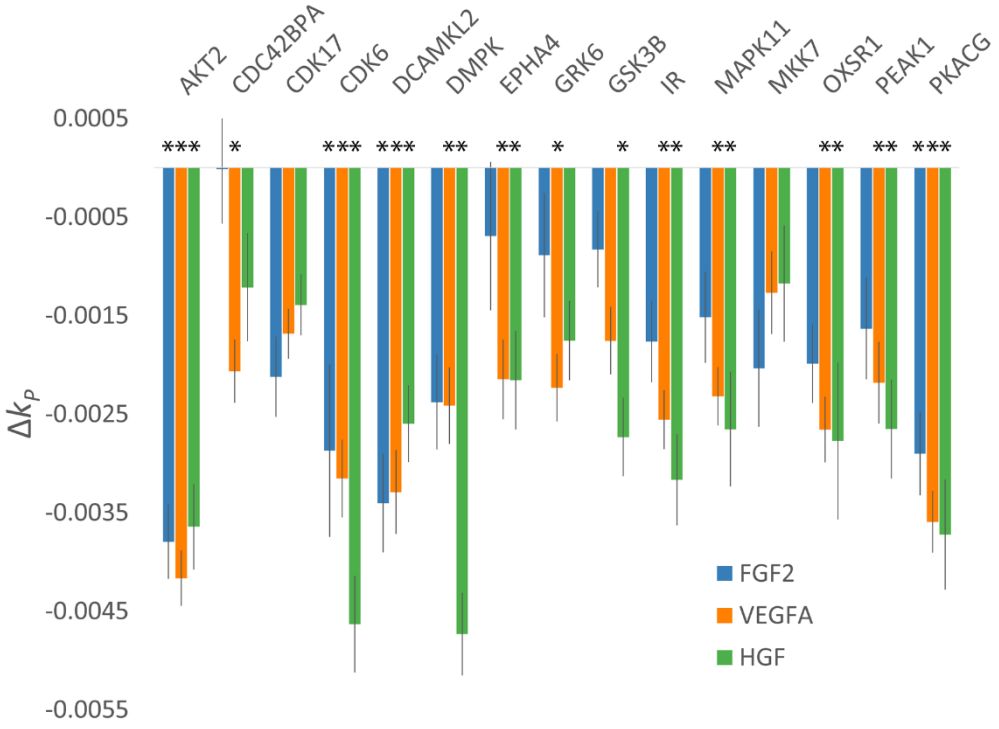
AKT2
CDC42BPA
CDK17
CDK6
DCAMKL2
DMPK
EPHA4
GRK6
GSK3B
IR
MAPK11
MKK7
OXSR1
PEAK1
PKACG
Δk_p
0.0005
-0.0005
-0.0015
-0.0025
-0.0035
-0.0045
-0.0055
FGF2
VEGFA
HGF

TABLE S1

Growth Factor	Supplier	MW (kDa)	Highest Concentration Tested (nM)	Pro-Proliferative?
Activin A	PeproTech	26	3.85	N
Ang1	PeproTech	56.3	1.78	N
Ang2	PeproTech	50.1	2	N
CTGF	PeproTech	11	9.09	N
EG-VEGF	PeproTech	9.6	10.42	N
EGF	Millipore	133.95	0.01	Y (weak)
FGF1	PeproTech	16.8	5.95	Y
FGF2	PeproTech	17.2	5.81	Y
FGF3	R&D	21.1	7.11	N
G-CSF	PeproTech	18.7	5.35	N
GM-CSF	PeproTech	14.6	13.7	N
Heregulin 1	PeproTech	7.5	13.33	N
HGF	PeproTech	79.4	2.52	Y
IGF-1	R&D	7.6	26.32	N
IL-1β	R&D	17.3	5.78	N
IL8	PeproTech	8.9	11.24	N
Leptin	R&D	16	62.5	N
MCP-1	PeproTech	8.6	11.63	N
PDGF-BB	R&D	24.3	4.12	N
PlGF	PeproTech	29.7	5.05	N
SDF-1α	PeproTech	8	25	N
TGF-α	PeproTech	5.5	18.18	Y (weak)
TGF-β1	PeproTech	25	4	N
TGF-β2	PeproTech	25	4	N
TGF-β3	PeproTech	25	4	N
VEGFA 121	R&D	28	5.36	Y (weak)
VEGFA 145	R&D	34	4.41	Y
VEGFA 165	PeproTech	38.2	3.93	Y
VEGF B	PeproTech	38	3.95	N
VEGF C	PeproTech	27	5.56	N
VEGF D	PeproTech	26.2	5.73	N
Wnt1	PeproTech	38.4	2.6	N
Wnt7B	PeproTech	35.5	2.82	N

FIGURE S1

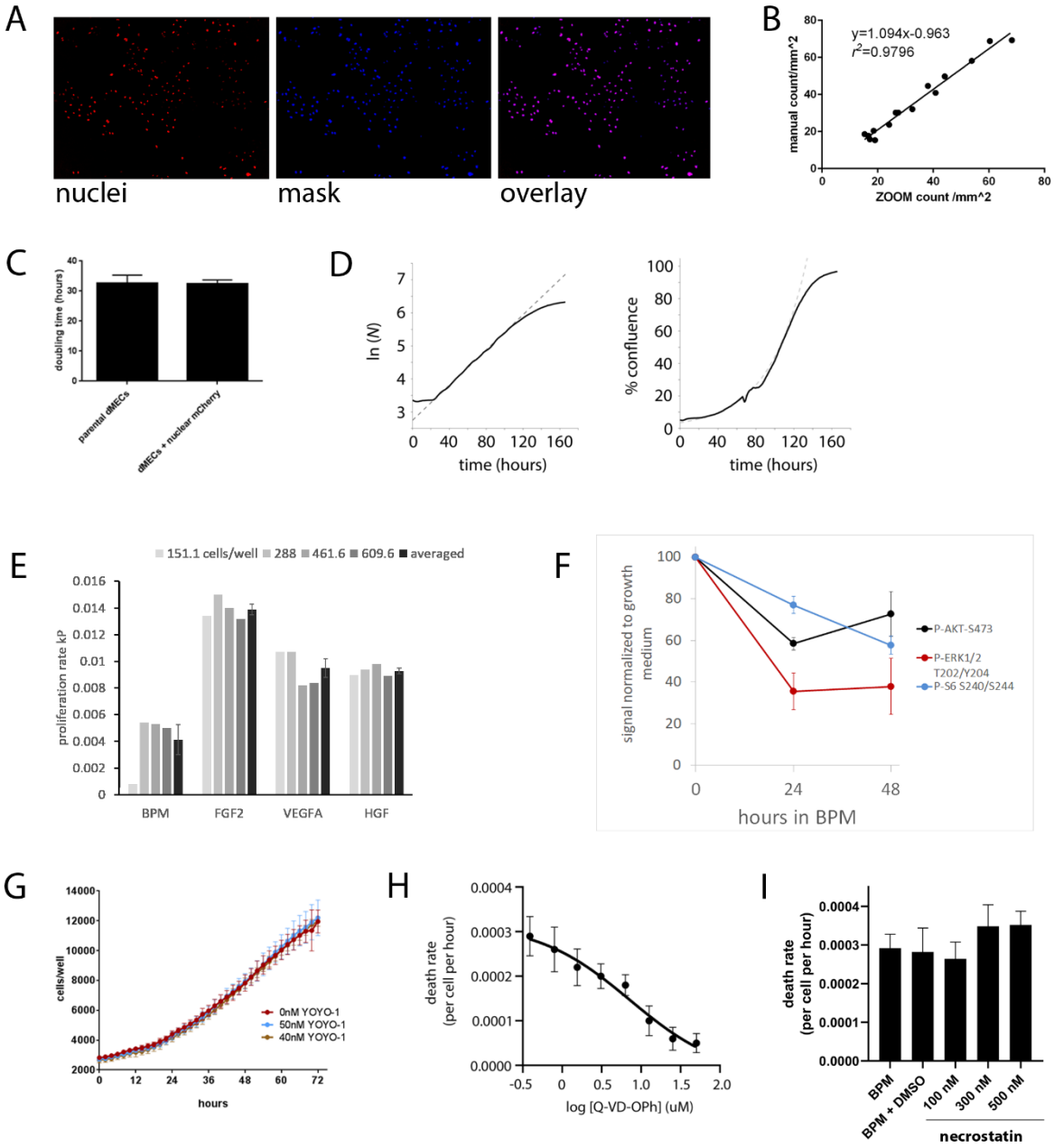
A
nuclei
mask
overlay
B
y=1.094x-0.963
r2=0.9796
manual count/mm^2
ZOOM count /mm^2
C
doubling time (hours)
parental dMECs
dMECs + nuclear mCherry
D
ln (N)
time (hours)
% confluence
time (hours)
E
151.1 cells/well
288
461.6
609.6
averaged
proliferation rate kP
BPM
FGF2
VEGFA
HGF
F
signal normalized to growth medium
P-AKT-S473
P-ERK1/2 T202/Y204
P-S6 S240/S244
hours in BPM
G
cells/well
0nM YOYO-1
50nM YOYO-1
40nM YOYO-1
hours
H
death rate (per cell per hour)
log [Q-VD-OPh] (uM)
I
death rate (per cell per hour)
BPM
BPM + DMSO
100 nM
300 nM
500 nM
necrostatin

FIGURE S2

A

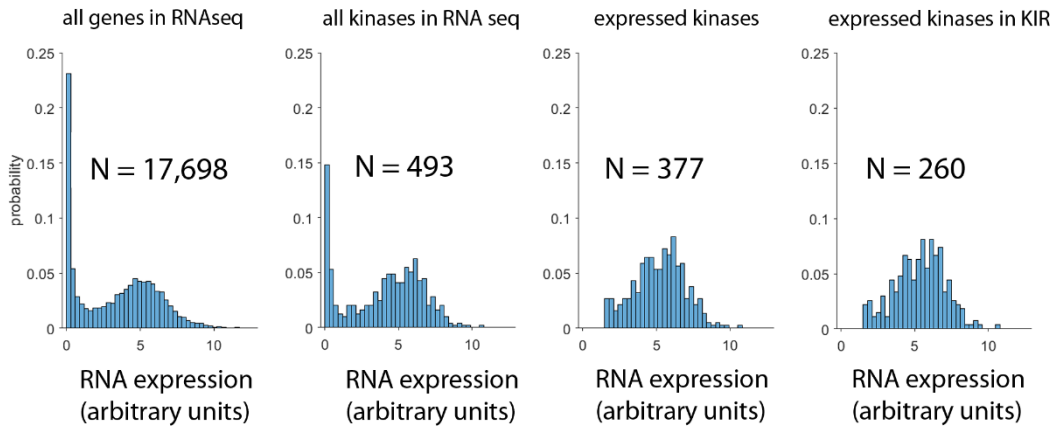
all genes in RNAseq
all kinases in RNA seq
expressed kinases
expressed kinases in KIR
probability
N = 17,698
N = 493
N = 377
N = 260
RNA expression (arbitrary units)
RNA expression (arbitrary units)
RNA expression (arbitrary units)
RNA expression (arbitrary units)

B

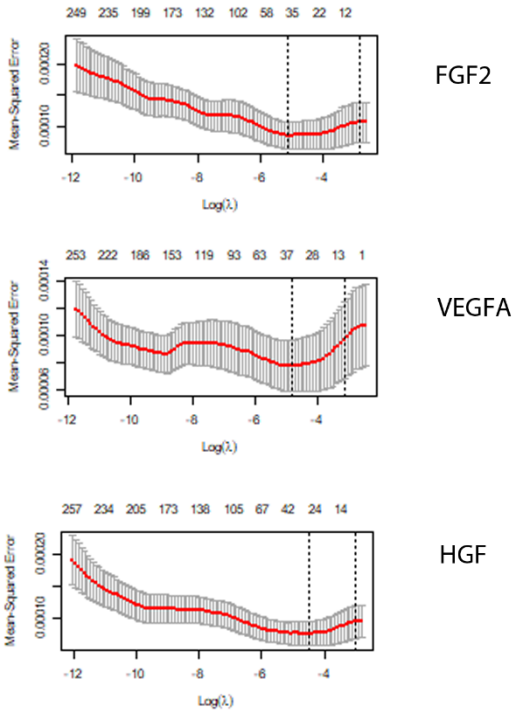
249 235 199 173 132 102 58 35 22 12
FGF2
253 222 186 153 119 93 63 37 28 13 1
VEGFA
257 234 205 173 138 105 67 42 24 14
HGF
Mean-Squared Error
Log(λ)

FIGURE S3

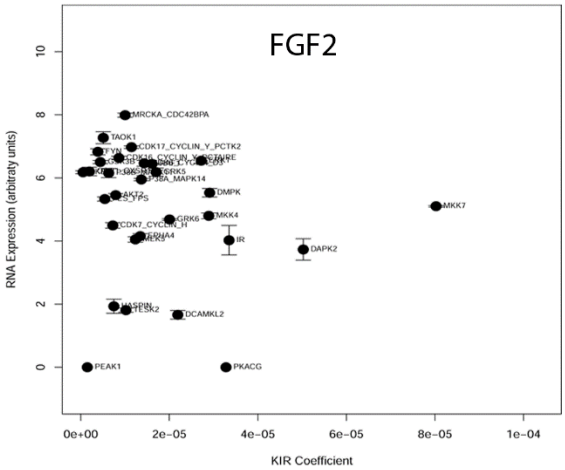
FGF2
RNA Expression (arbitraty units)
KIR Coefficient
MRCKA_CDC42BPA
TAOK1
CDK17_CYCLIN_Y_PCTK2
DMPK
MKK7
MKK4
IR
DAPK2
DCAMKL2
PEAK1
PKACG

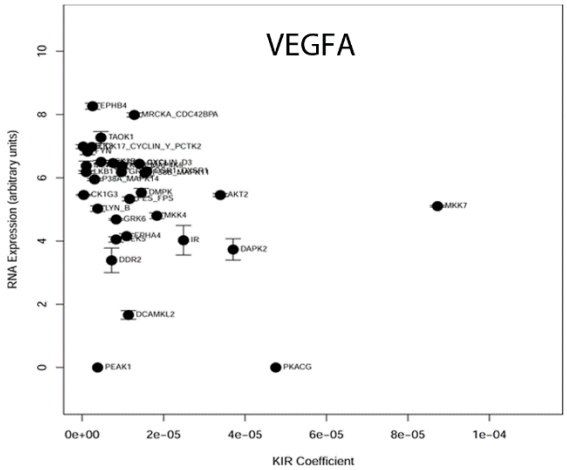
VEGFA
RNA Expression (arbitrary units)
KIR Coefficient
EPHB4
MRCKA_CDC42BPA
TAOK1
CDK17_CYCLIN_Y_PCTK2
AKT2
MKK7
MKK4
IR
DAPK2
DDR2
DCAMKL2
PEAK1
PKACG

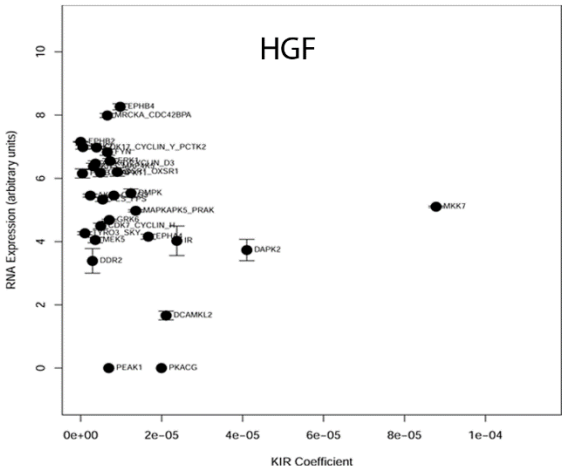
HGF
RNA Expression (arbitrary units)
KIR Coefficient
EPHB4
MRCKA_CDC42BPA
MAPKAPK5_PRAK
MKK7
IR
DAPK2
DDR2
DCAMKL2
PEAK1
PKACG

FIGURE S4

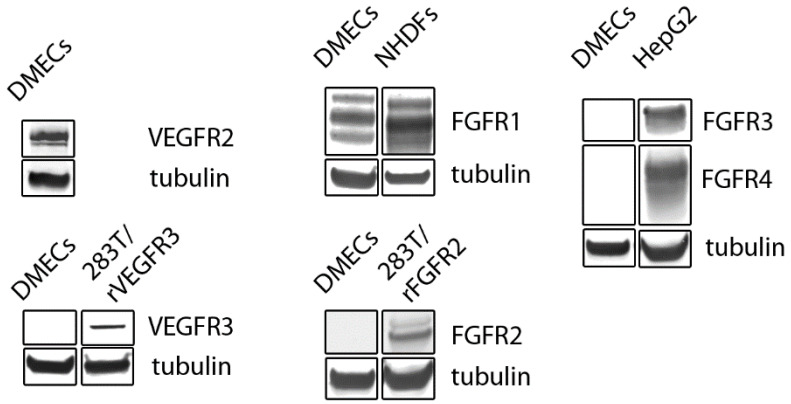
DMECs
VEGFR2
tubulin
DMECs
NHDFs
FGFR1
tubulin
DMECs
HepG2
FGFR3
FGFR4
tubulin
DMECs
283T/
rVEGFR3
VEGFR3
tubulin
DMECs
283T/
rFGFR2
FGFR2
tubulin

References

Cabral, Thiago, Luiz Guilherme M. Mello, Luiz H. Lima, Júlia Polido, Caio V. Regatieri, Rubens Belfort Jr, and Vinit B. Mahajan. 2017. "Retinal and Choroidal Angiogenesis: A Review of New Targets." *International Journal of Retina and Vitreous* 3 (August): 31.

Carmeliet, Peter. 2005. "VEGF as a Key Mediator of Angiogenesis in Cancer." *Oncology* 69 Suppl 3 (November): 4–10.

Chandrakesan, Parthasarathy, Jiannan Yao, Dongfeng Qu, Randal May, Nathaniel Weygant, Yang Ge, Naushad Ali, et al. 2017. "Dclk1, a Tumor Stem Cell Marker, Regulates pro-Survival Signaling and Self-Renewal of Intestinal Tumor Cells." *Molecular Cancer* 16 (1): 30.

Choueiri, Toni K., Bernard Escudier, Thomas Powles, Paul N. Mainwaring, Brian I. Rini, Frede Donskov, Hans Hammers, et al. 2015. "Cabozantinib versus Everolimus in Advanced Renal-Cell Carcinoma." *The New England Journal of Medicine* 373 (19): 1814–23.

Collins, M. K., G. R. Perkins, G. Rodriguez-Tarduchy, M. A. Nieto, and A. López-Rivas. 1994. "Growth Factors as Survival Factors: Regulation of Apoptosis." *BioEssays: News and Reviews in Molecular, Cellular and Developmental Biology* 16 (2): 133–38.

Crawford, Talia N., D. Virgil Alfaro 3rd, John B. Kerrison, and Eric P. Jablon. 2009. "Diabetic Retinopathy and Angiogenesis." *Current Diabetes Reviews* 5 (1): 8–13.

Davis, Carrie A., Benjamin C. Hitz, Cricket A. Sloan, Esther T. Chan, Jean M. Davidson, Idan Gabdank, Jason A. Hilton, et al. 2018. "The Encyclopedia of DNA Elements (ENCODE): Data Portal Update." *Nucleic Acids Research* 46 (D1): D794–801.

Ehab, Moataz, and Mohamad Elbaz. 2016. "Profile of Palbociclib in the Treatment of Metastatic Breast Cancer." *Breast Cancer* 8 (May): 83–91.

ENCODE Project Consortium. 2012. "An Integrated Encyclopedia of DNA Elements in the Human Genome." *Nature* 489 (7414): 57–74.

Ferguson, Fleur M., Behnam Nabet, Srivatsan Raghavan, Yan Liu, Alan L. Leggett, Miljan Kuljanin, Radha L. Kalekar, et al. 2020. "Discovery of a Selective Inhibitor of Doublecortin like Kinase 1." *Nature Chemical Biology* 16 (6): 635–43.

Grépin, Renaud, and Gilles Pagès. 2010. "Molecular Mechanisms of Resistance to Tumour Anti-Angiogenic Strategies." *Journal of Oncology* 2010 (March). https://doi.org/10.1155/2010/835680.

Gross, Sean M., and Peter Rotwein. 2016. "Unraveling Growth Factor Signaling and Cell Cycle Progression in Individual Fibroblasts." *The Journal of Biological Chemistry* 291 (28): 14628–38.

Grünwald, Viktor, and Axel Stuart Merseburger. 2013. "The Progression Free Survival-Plateau with Vascular Endothelial Growth Factor Receptor Inhibitors – Is There More to Come?" *European Journal of Cancer* 49 (11): 2504–11.

Gujral, Taranjit S., Marina Chan, Leonid Peshkin, Peter K. Sorger, Marc W. Kirschner, and Gavin MacBeath. 2014. "A Noncanonical Frizzled2 Pathway Regulates Epithelial-Mesenchymal Transition and Metastasis." *Cell* 159 (4): 844–56.

Gujral, Taranjit Singh, Leonid Peshkin, and Marc W. Kirschner. 2014. "Exploiting Polypharmacology for Drug Target Deconvolution." *Proceedings of the National Academy of Sciences of the United States of America* 111 (13): 5048–53.

Hsieh, James J., Mark P. Purdue, Sabina Signoretti, Charles Swanton, Laurence Albiges, Manuela Schmidinger, Daniel Y. Heng, James Larkin, and Vincenzo Ficarra. 2017. "Renal Cell Carcinoma." *Nature Reviews. Disease Primers* 3 (March): 17009.

Jászai, József, and Mirko H. H. Schmidt. 2019. "Trends and Challenges in Tumor Anti-Angiogenic Therapies." *Cells* 8 (9): 1102.

Khan, Kabir A., and Roy Bicknell. 2016. "Anti-Angiogenic Alternatives to VEGF Blockade." *Clinical & Experimental Metastasis* 33 (2): 197–210.

Letai, Anthony. 2006. "Growth Factor Withdrawal and Apoptosis: The Middle Game." *Molecular Cell* 21 (6): 728–30.

Liu, Minghui, Hongyu Liu, and Jun Chen. 2018. "Mechanisms of the CDK4/6 Inhibitor Palbociclib (PD 0332991) and Its Future Application in Cancer Treatment (Review)." *Oncology Reports* 39 (3): 901–11.

Mollica, Veronica, Vincenzo Di Nunno, Lidia Gatto, Matteo Santoni, Marina Scarpelli, Alessia Cimadamore, Antonio Lopez-Beltran, et al. 2019. "Resistance to Systemic Agents in Renal Cell

Carcinoma Predict and Overcome Genomic Strategies Adopted by Tumor." *Cancers* 11 (6). https://doi.org/10.3390/cancers11060830.
Nawabi, Homaira, Stephane Belin, Romain Cartoni, Philip R. Williams, Chen Wang, Alban Latremolière, Xuhua Wang, et al. 2015. "Doublecortin-Like Kinases Promote Neuronal Survival and Induce Growth Cone Reformation via Distinct Mechanisms." *Neuron* 88 (4): 704–19.
Potente, Michael, Holger Gerhardt, and Peter Carmeliet. 2011. "Basic and Therapeutic Aspects of Angiogenesis." *Cell* 146 (6): 873–87.
Rata, Scott, Jonathan Scott Gruver, Natalia Trikoz, Alexander Lukyanov, Janelle Vultaggio, Michele Ceribelli, Craig Thomas, Taran Singh Gujral, Marc W. Kirschner, and Leonid Peshkin. 2020. "An Optimal Set of Inhibitors for Reverse Engineering via Kinase Regularization." *Cold Spring Harbor Laboratory*. https://doi.org/10.1101/2020.09.26.312348.
Sarkar, Siddik, and Mahitosh Mandal. 2009. "Growth Factor Receptors and Apoptosis Regulators: Signaling Pathways, Prognosis, Chemosensitivity and Treatment Outcomes of Breast Cancer." *Breast Cancer: Basic and Clinical Research* 3 (August): 47–60.
Sherr, Charles J., David Beach, and Geoffrey I. Shapiro. 2016. "Targeting CDK4 and CDK6: From Discovery to Therapy." *Cancer Discovery* 6 (4): 353–67.
Shiojima Ichiro, and Walsh Kenneth. 2002. "Role of Akt Signaling in Vascular Homeostasis and Angiogenesis." *Circulation Research* 90 (12): 1243–50.
Srinivasan, Ruchika, Tahera Zabuawala, Hong Huang, Jianying Zhang, Parul Gulati, Soledad Fernandez, J. Colleen Karlo, Gary E. Landreth, Gustavo Leone, and Michael C. Ostrowski. 2009. "Erk1 and Erk2 Regulate Endothelial Cell Proliferation and Migration during Mouse Embryonic Angiogenesis." *PloS One* 4 (12): e8283.
Veríssimo, André, Eunice Carrasquinha, Marta B. Lopes, Arlindo L. Oliveira, Marie-France Sagot, and Susana Vinga. 2018. "Sparse Network-Based Regularization for the Analysis of Patientomics High-Dimensional Survival Data." *Cold Spring Harbor Laboratory*. https://doi.org/10.1101/403402.
Wang, Huawei, John Lapek, Ken Fujimura, Jan Strnadel, Bei Liu, David J. Gonzalez, Wei Zhang, et al. 2018. "Pseudopodium-Enriched Atypical Kinase 1 Mediates Angiogenesis by Modulating GATA2-Dependent VEGFR2 Transcription." *Cell Discovery* 4 (1): 26.
Yang, Jie, Qing-Dong Shi, Tian-Bao Song, Gai-Feng Feng, Wei-Jing Zang, Chang-Hong Zong, and Ling Chang. 2013. "Vasoactive Intestinal Peptide Increases VEGF Expression to Promote Proliferation of Brain Vascular Endothelial Cells via the CAMP/PKA Pathway after Ischemic Insult in Vitro." *Peptides* 42 (April): 105–11.
Zetterberg, A., and O. Larsson. 1985. "Kinetic Analysis of Regulatory Events in G1 Leading to Proliferation or Quiescence of Swiss 3T3 Cells." *Proceedings of the National Academy of Sciences of the United States of America* 82 (16): 5365–69.
Zhou, L., X-D Liu, M. Sun, X. Zhang, P. German, S. Bai, Z. Ding, et al. 2016. "Targeting MET and AXL Overcomes Resistance to Sunitinib Therapy in Renal Cell Carcinoma." *Oncogene* 35 (21): 2687–97.